Behavioral/Cognitive

Two Functionally Distinct Serotonergic Projections into Hippocampus

Alessandro Luchetti,[1,2] **Ayaka Bota,**[1,3,4] **Adam Weitemier,**[1,5] **Kotaro Mizuta,**[1,3] **Masaaki Sato,**[1,5,6] **Tanvir Islam,**[1,5] **Thomas J. McHugh,**[1,5] **Ayumu Tashiro,**[2] **and Yasunori Hayashi**[1,3,6]

[1]RIKEN Brain Science Institute, Wako, 351-0198, Japan, [2]School of Biological Sciences, Nanyang Technological University, Singapore, 308232, [3]Kyoto University Graduate School of Medicine, Kyoto, 606-8501, Japan, [4]Graduate School of Science and Engineering, Saitama University, Saitama, 338-8570, Japan, [5]RIKEN Center for Brain Science, Wako, 351-0198, Japan, and [6]Brain and Body System Science Institute, Saitama University, Saitama, 338-8570, Japan

Hippocampus receives dense serotonergic input specifically from raphe nuclei. However, what information is carried by this input and its impact on behavior has not been fully elucidated. Here we used *in vivo* two-photon imaging of activity of hippocampal median raphe projection fibers in behaving male and female mice and identified two distinct populations: one linked to reward delivery and the other to locomotion. Local optogenetic manipulation of these fibers confirmed a functional role for these projections in the modulation of reward-induced behavior. The diverse function of serotonergic inputs suggests a key role in integrating locomotion and reward information into the hippocampal CA1.

Key words: **CA1; calcium imaging; in vivo; optogenetics; reward; serotonin**

Significance Statement

Information constantly flows in the hippocampus, but only some of it is captured as a memory. One potential process that discriminates which information should be remembered is concomitance with reward. In this work, we report a neuromodulatory pathway, which delivers reward signal as well as locomotion signal to the hippocampal CA1. We found that the serotonergic system delivers heterogeneous input that may be integrated by the hippocampus to support its mnemonic functions. It is dynamically involved in regulating behavior through interaction with the hippocampus. Our results suggest that the serotonergic system interacts with the hippocampus in a dynamic and behaviorally specific manner to regulate reward-related information processing.

Introduction

Serotonergic systems show anatomic heterogeneity in their source nuclei and afferent projections. As such, they can modulate a variety of brain functions (Lesch and Waider, 2012). The major source of forebrain serotonergic fibers, the dorsal raphe (composed of B6 and B7 subnuclei), projects to the structures, including the basal ganglia, PFC, septum, and amygdala (Azmitia and Segal, 1978; Gauthier and Tank, 2018). The activity of the dorsal raphe has been linked to a variety of behaviors, including anxiety, pain, spatial memory, reward-seeking, and increased patience (Dugue et al., 2014; Liu et al., 2014; Miyazaki et al., 2014; Ohmura et al., 2014; Li et al., 2016; Teixeira et al., 2018). The median raphe (nucleus centralis superior, B5 and B8 subnuclei), projects mainly to midline structures, including the tegmental nucleus, interpeduncular nucleus, mammillary body, supramammillary nucleus, hypothalamus, thalamus, lateral habenula, diagonal band nuclei, medial septum, and hippocampal formation (Kohler and Steinbusch, 1982; Vertes et al., 1999). Existing studies have linked median raphe activity to theta rhythm, aversive stimuli, sleep, and memory processing (Kocsis et al., 2006; Jackson et al., 2008; Wang et al., 2015; Domonkos et al., 2016). These two projections are largely nonoverlapping.

Received Nov. 13, 2019; revised Apr. 12, 2020; accepted May 10, 2020.

Author contributions: A.L. and Y.H. designed research; A.L., A.B., and A.W. performed research; A.L., T.I., A.T., and Y.H. analyzed data; A.L. wrote the first draft of the paper; A.L., A.B., A.W., K.M., T.J.M., A.T., and Y. H. edited the paper; A.L. and Y.H. wrote the paper; K.M., M.S., T.I., and T.J.M. contributed unpublished reagents/analytic tools.

A.L. received a Japan Society for the Promotion of Science Postdoctoral Fellowship for Foreign Researchers and Japan Society for the Promotion of Science Grant-in-Aid for Japan Society for the Promotion of Science Fellows (15F14409). This work was supported by RIKEN, RIKEN Presidents Fund, Grant-in-Aid for Scientific Research (A, 20240032, 16H02455) and for Scientific Research on Innovative Area "Foundation of Synapse and Neurocircuit Pathology" (22110006) and "Constructive understanding of multi-scale dynamism of neuropsychiatric disorders" (18H05434) from the MEXT, Japan, Human Frontier Science Program, Uehara Memorial Foundation, Naito Foundation, Takeda Science Foundation, Japan Foundation for Applied Enzymology, Novartis Foundation (Japan) for the Promotion of Science, Research Foundation for Opto-Science and Technology, and Brain Science Foundation to Y.H. This work was also supported by Ministry of Education, Singapore, AcRF Tier 2 (MOE2015-T2-2-035), and National Medical Research Council, Singapore, OF-IRG (NMRC/OFIRG/0046/2017-00). We thank Drs. Kota Tamada and Toru Takumi for sharing unpublished data and materials.

A. Luchetti's present address: Brain Research Institute, University of California at Los Angeles, Los Angeles, CA 90095.

Y.H. received research fund from Fujitsu Laboratories and Dwango. The remaining authors declare no competing financial interests.

Correspondence should be addressed to Yasunori Hayashi at yhayashi-tky@umin.ac.jp.

https://doi.org/10.1523/JNEUROSCI.2724-19.2020

This anatomic heterogeneity is consistent with the divergent functions of serotonergic system.

The hippocampus, a fundamental structure for spatial and temporal learning (Eichenbaum, 2000), receives heterogeneous serotonergic inputs. The fibers mainly originate from the median raphe, where they are known to form synapses on various types of interneurons in the hippocampal circuit (Kohler and Steinbusch, 1982; Papp et al., 1999; Vertes et al., 1999; Varga et al., 2009; Turi et al., 2019). In addition, the caudal and interfascicular subnucleus of the dorsal raphe also project to the hippocampus (Vertes, 1991; McKenna and Vertes, 2001; Izawa et al., 2019). Given this anatomic heterogeneity, the possibility that serotonergic inputs to the hippocampus may play multiple functional roles highlights the importance of actually monitoring the activity of these inputs during behavior. Indeed, while existing evidence points to a role of the median raphe-hippocampal serotonergic projections in memory (Wang et al., 2015; Fernandez et al., 2017; Teixeira et al., 2018), the firing properties of these inputs and their functional roles remain elusive. We predict that a diverse range of information would need to be carried by the serotonergic system to explain its involvement in such a wide variety of behaviors.

In order to shed light on the role of serotonergic input to the hippocampus, we investigated the activity of serotonergic fibers within the dorsal hippocampal CA1 region via chronic *in vivo* Ca^{2+} imaging in mice behaving in virtual reality (VR). We found that the fibers consist of at least two functionally distinct populations: one firing on reward delivery and the other on the initiation of locomotion. Optogenetic inhibition of these fibers modulated the reward-induced behavioral changes in a goal-directed task. These differential functions of serotonergic inputs suggest that the serotonergic system plays a key role in integrating locomotion and reward information in hippocampal CA1.

Materials and Methods

Animals. All procedures conformed to the institutional guideline of RIKEN. Mice, 12–18 weeks old at the beginning of the experimental procedure, were housed with 1–4 cage-mates in a 12 h (8:00 AM to 8:00 PM) light/dark cycle, with food and water. *Sert-GFP* transgenic mice (*Tg(Slc6a4-EGFP)JP55Gsat*; Gensat) backcrossed 5 times to *C57BL/6J* were obtained from Kota Tamada and Toru Takumi. For Ca^{2+} imaging experiments, we used adult male and female mice heterozygous for the transgene *Sert-Cre (Tg(Slc6a4-cre)ET33Gsat*; Gensat) in the *C57BL/6J* background. For optogenetics experiments, we used male and female offspring obtained by crossing the *Sert-Cre* line with *Ai39 (Gt(ROSA)26Sortm39$^{(CAG-HOP/EYFP)Hze}$* JAX #014539).

Animals for in vivo *two-photon imaging of serotonergic inputs to the CA1.* A total of 7 mice were used for the 2-photon imaging experiments of serotonergic fibers in CA1. Mice received one 5 min session in the virtual linear track per day. All mice were trained between 1 and 4 d before the first imaging. This was necessary to find the location of a recordable fiber within the imaging window. Depending on the stability of the imaging window, the fibers were imaged over the course of 1-3 weeks of training, with 3-16 total sessions imaged per fiber. Animals were water-deprived for 2 d before beginning VR sessions. Both genders were used: 2 males and 1 female were used for the analysis of Type A fibers, and 1 male and 3 females were for Type B fibers.

Surgical procedure for in vivo *imaging.* Sert-Cre mice were anesthetized using isoflurane (3% induction, 1.5% maintenance) and placed in a stereotactic frame. The mice were injected with an adeno-associated virus (AAV) vector carrying a genetically encoded calcium sensor GCaMP6f (*AAV9.CAG.Flex.GCaMP6f.WPRE.SV40* concentration 5-$\times 10^{12}$ genome copy/ml from Penn Vector Core) targeted to the raphe nuclei. The procedure consisted of four injection sites. The injection coordinates were ML 1.5 mm at 10° angle to the skull on the mediolateral axis pointing medially, two injections at AP −4.5 mm from bregma, DV 3.5 and 4.0 mm from brain surface; and two injections at AP −5.0 mm from bregma, DV 3.5 and 4.0 mm from brain surface.

After virus injection, a stainless-steel headplate was implanted on the head of the animal. The plate was designed to allow animal head fixation and had a 7-mm-diameter opening to allow access to the skull. The location of the plate was centered roughly over the left hippocampus, and the plate was secured with dental acrylic.

One week after the headplate implantation, the animals underwent an additional surgery for the excavation of a small area of cortex overlying the dorsal CA1 and implantation of an imaging window consisting of a stainless-steel ring with a glass bottom (2.0 mm diameter, 0.15 mm thick). This window was targeted to the dorsal CA1 (centered at AP −2.0 mm from bregma, ML −2.0 mm). After the surgery, the animals were returned to their home cages and allowed to rest for 3 weeks before imaging.

Surgical procedure for optogenetic manipulation. For optogenetic manipulation, a similar surgical procedure was used as the one described above but without virus injection. *Sert-Cre/Ai39* line mice were implanted with the same type of stainless-steel headplate, and an optic cannula was then implanted over dorsal CA1 regions of both hemispheres. The coordinates used for the cannula implantation were AP −2.0 mm from bregma, ML 1.7 mm both sides, and DV 1.0 mm from the surface of the skull. Cannulas were then secured with dental acrylic and covered with a removable cap.

Two-photon microscopic imaging. To image the serotonergic projections to the CA1, mice were briefly anesthetized to clean the imaging window and head-fixed under the two-photon microscope (Nikon A1MP microscope equipped with a 16× NA 0.8 objective). The laser used for excitation was Ti:Sapphire laser (Mai Tai DeepSee eHP, Spectra-Physics) at 910 nm, and time-series fluorescence changes were imaged using a 495-540 nm bandpass filter and a GaAsP photomultiplier tube. The laser power under the objective was 10-20 mW. Images were acquired at a frequency of 7 Hz.

Raw videos were motion-corrected using ImageJ TurboReg image registration plug-in, and a ROI was manually drawn around the imaged fiber. Activity trace was obtained by detecting the average fluorescence of the ROI across all frames, subtracting the background and applying a 5 frame moving average. Baseline for graphs was calculated as the average fluorescence in the 2 s preceding each reward event or the −3 to −1 s preceding each run start. Stop events graphs baseline was calculated as the 2 s preceding each stop event.

Immunostaining. Mice were perfused with 4% PFA in PBS. Brain were removed and coronal sections were cut using a miscroslicer at 50 µm. The sections were incubated overnight with rabbit anti-serotonin transporter antibody (1:500, AB9726, Sigma Millipore), diluted in PBS containing 2% normal goat serum, 1% BSA, and 0.1% Triton X-100, followed by AlexaFluor-594-labeled goat anti-rabbit IgG antibody (1:1000, A-11 032 or A-11 037, Thermo Fisher Scientific) and Hoechst 33258 (1:1000, #382061, Calbiochem). The GCaMP signal shown in all the images represents native fluorescence. Fluorescence images were acquired using a Keyence BZ-9000 epifluorescence microscope equipped with a 4× objective (Keyence) or an Olympus FV1000 laser-scanning confocal microscope equipped with a 60× water immersion objective (Olympus).

VR setup. The VR setup consisted of a head-fixed setup in which mice could run on a cylinder; ~30 cm in front of the mouse, a single widescreen LCD screen (Dell U2313) displayed a moving track, and a cannula delivered water rewards to the animals. The virtual track was rendered using OmegaSpace 3.1 (Solidray) running on a Windows 7 computer in 81° horizontal and 51° vertical FOVs. Rotations of the cylinder were detected by an USB optical mouse (Logitech G400) placed in proximity of the cylinder itself. The USB mouse controlled the movements of the VR track using custom drivers and custom-made software in LabVIEW (National Instruments). Water rewards were controlled by VR track position and delivered using a pump (O'Hara).

Behavior under VR. After recovery from surgery, mice were habituated to the experimenters by 5 d of handling sessions lasting 10 min each. During these sessions, mice were also habituated to walk on a

Styrofoam ball (20 cm in diameter) without being head-fixed. The ball was turned manually as the animal climbed around it. After this habituation, mice were water-deprived for 2 d and then began the regimen of the VR linear track, one session per day. During the VR experiments, mice were head-fixed over the Styrofoam cylinder (20 cm in diameter and 10 cm in width) and began running on the track. The virtual linear track was 120 cm long, appearing as a corridor with black and white walls, gray sky, and several cues outside the corridor. The mouse was only allowed to move straight in the track. Global cues were present in the distance within the VR track as well as proximal cues. In order to find the fibers to record, the mice had to be awake and behaving. For this reason, the first sessions of each animal in the VR were used to locate a fiber to record before daily imaging began. Between one and four sessions were spent to identify the location of a fiber. Recording of the fiber was then performed every day as long as the window and imaging conditions were maintained. Imaging sessions during the VR task lasted 5 min to minimize potential photograph-bleaching of the imaged fiber.

Larger reward and satiety response tests. One reward fiber was tested during either unpredicted water reward receipt, or enhanced reward receipt (10 rewards instead of 1). The single unpredicted rewards were delivered while the animal was not moving, to avoid locomotion effects related to the animal stopping running to drink. At the end of these sessions, the animal was allowed to drink water *ad libitum* in the home cage until the next day. Then the animal was tested in the same paradigm to observe activity of the fiber under satiety.

Data analysis. For quantification of mouse slowdown and halt, as well as water reward receipt, we used data from well-trained animals (all 7 imaged animals, day 7 of training). Delay was measured between water receipt and full stop (0 speed, 2 s timeout). The delay between reward receipt and 50% of the deceleration was also measured. Water reward receipt was measured as the number of water rewards received by the animals.

Because of the sparsity of detected fibers, we rarely found more than one fiber per FOV. Even in cases where we could see multiple fibers at once, we focused one fiber in a session because it was difficult to judge whether any two fibers are from two different cells or branches from single cells. Traces for the fiber average fluorescence were calculated by averaging all session for all imaged fiber of that type. Reward location was identified as frames in which the mouse received a water reward. Since the VR track is designed to deliver up to three reward drops in succession, only the first of the reward point per lap was used for activity averaging. Initiation of locomotion was detected as at least 3 s of movement (average speed above 1 cm/s) preceded by at least 2 s of immobility (speed at 0 cm/s). Speed average traces were generated in the same way, and represent the average speed averaged at event. For individual session traces, the average was calculated across events within that session.

Comparisons against randomized data were performed by creating 1000 reshuffling of each fluorescent trace by shifting the fluorescence sequence by a random amount within each lap (every lap was reshuffled separately rather than the entire trace). The δ for reward and run-start were then measured using these randomized traces, and the means compared against the real data.

Stop points were identified as at least 2 s of continuous immobility (speed at 0 cm/s) preceded by at least 3 s of locomotion (average speed above 1 cm/s). Analysis of activity at stopping was performed using trials in which the animals were voluntarily running in the VR setup without any visual input or any reward delivered.

To assess the average fluorescence during ongoing locomotion and immobility, we excluded frames near events of run-start (1 s before and 1.5 s after) and reward (3 s after). The rest of the frames were pooled and averaged for the session. For high-activity (peak) analysis, we identified the top 5% intensity frames and then measured their frequency within locomotion, immobility, reward, and run-start.

To attempt separating locomotion activity from reward activity in Type B fibers, reward-only points were detected as times in which the animal received a water reward without identified stop points or run-start points 3 s before or after the reward time.

Detection of start and peak of event-related calcium activity was calculated by scanning 1.5 s before and after the events (reward for Type A fibers, run-start for Type B fibers) and identifying the highest activity as peak. The start of the peak was detected as two consecutive frames of the fluorescence raising above the baseline fluorescence. Sessions where the peak preceded the event were excluded. These are sessions from mice performing the VR linear track as described above.

Individual calculation of δ fluorescence before the events was done by averaging fluorescence 2 s before and 2 s after reward receipt or stop event; and -3 to -1 s before against -1 to $+1$ s for run-start.

Optogenetics. A total of 12 mice, 7 double transgenic *Sert-Cre/Ai39* mice (2 males and 5 females) and 5 single-transgenic control littermate mice (3 males and 2 females), carrying either one or none of the transgene, were used. Mice underwent a similar paradigm as described before. Water-deprived animals received one 10 min session per day in the virtual linear track. Mice received a water drop reward on entering the reward zone and up to two more drops if they remained in the reward zone for up to 2 s longer. At the end of the track, animals were teleported back to the start after a 1 s delay. The laser was active while the animal was in the reward zone, and off outside of it. We used a 593 nm laser at 10 mW with continuous illumination.

Behavioral outputs were tracked by custom LabVIEW software and analyzed using MATLAB at a frequency of 50 Hz. Percentage of error trials was calculated as the number of trials where the animals failed to collect all three rewards, divided by the number of laps. Rewards per lap were calculated as the total rewards collected divided by the total laps performed by the animal during a session. Spatial occupancy was calculated by dividing the linear track in 20 bins after trimming the extremities of the track (2% at the borders at which the track starts and ends/resets). Number of frames spent within each bin were then added up and converted into time spent for that trial and that animal. Halt in reward zone was measured as the average duration of the animal's halting in the reward zone for each session. Sessions were excluded from the analysis if a mouse completed <3 laps in 10 min or if no rewards were collected across the entire 10 min session.

Experimental design and statistical analysis. Data are expressed as the mean $\pm$ SEM unless stated otherwise. All *t* tests are two-tailed unless specified. Normal distribution of means was tested using *F* test. Significance levels were set to $p = 0.05$. Sidak correction was applied to all multiple comparisons unless specified. Outlier data points were detected using the method of interquartile range. No statistical methods were used to predetermine sample size. Sample sizes were chosen on the basis of previous studies. Statistical tests were performed using SPSS (IBM) and GraphPad Prism version 6.01 (GraphPad).

Results

Heterogeneity of serotonergic projections in CA1

We first attempted to visualize the distribution of serotonergic fibers in the dorsal hippocampus in live mice. For this purpose, we implanted an optical window over the dorsal hippocampus by removing a part of overlaying cortex of *Sert-GFP* transgenic animal, which expresses GFP under the control of serotonin transporter (*Slc6a4*) promotor (Fig. 1*A*). Using a two-photon microscope, we could find fibers in all layers of dorsal hippocampus from stratum oriens to the upper portion of stratum radiatum, after which the signal from the fibers was too dim for visualization (Fig. 1*B*). This distribution of serotonergic fibers in the dorsal hippocampus is largely consistent with previous literatures visualizing serotonin immunoreactivity in fixed tissues (Ihara et al., 1988).

In order to monitor the activity of these serotonergic projections in live mice, we conducted Ca^{2+} imaging using GCaMP6f. We initially tested *Ai95(RCL-GCaMP6f)-D* (with floxed *GCaMP6f* locus) animals crossed with *Sert-Cre* animals. However, the fluorescent level was too weak for prolonged imaging. Therefore, we

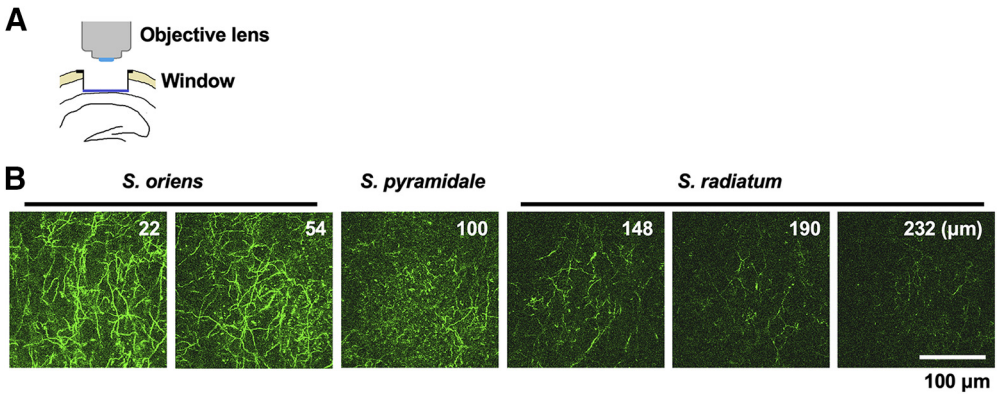

Figure 1. Distribution of serotonergic fibers in dorsal hippocampus. ***A***, Imaging scheme. A part of overlaying cortex was removed, and an optical window was implanted, through which hippocampus could be observed under two-photon microscope. ***B***, Serotonergic fibers in Sert-GFP transgenic mouse. The images were taken from the stratum oriens to the superficial portion of stratum radiatum using the same excitation and detection conditions. The numbers indicate depth from alveus.

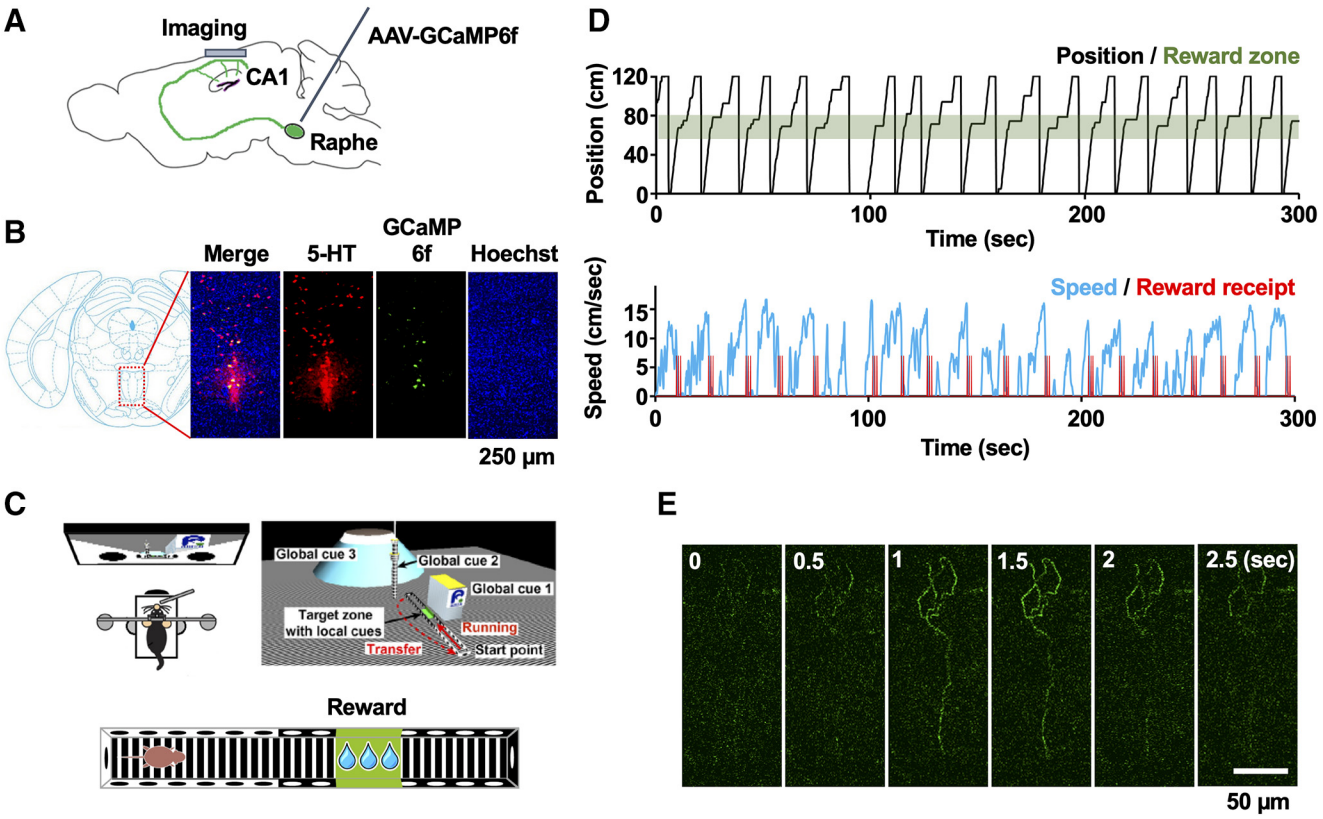

Figure 2. Imaging of serotonergic projections in CA1. ***A***, Injection of AAV vector-expressing calcium indicator GCaMP6f into raphe. ***B***, Representative histology of *Sert-Cre* mouse injected with floxed GCaMP6f virus. Diagram adapted from Paxinos and Franklin (2004). ***C***, Schematic drawing of the VR used in this study. ***D***, Representative example of animal's behavior in the virtual linear track and position (top), as well as speed and reward receipt (bottom). ***E***, Representative images of serotonergic fiber *in vivo* (see Movie 1).

turned to a Cre-inducible AAV vector expressing the calcium-sensitive indicator GCaMP6f (Fig. 2*A*). The vector was targeted to the median raphe in a transgenic mouse line expressing the Cre recombinase under the control of the serotonin transporter (*Sert-Cre* line) (Gong et al., 2003). As a result, 97.5 ± 1% of GCaMP6f-expressing cells were also immunopositive for serotonin and 16.2 ± 3.4% of cells immunopositive for serotonin expressed GCaMP6f ($n = 4$ mice) (Fig. 2*B*), demonstrating specific targeting of serotonergic neurons. It is important to note that, while neurons are known to release serotonin, some can also corelease glutamate (Szőnyi et al., 2016; Sos et al., 2017). Nonetheless, this approach allows us unprecedented detection of the activity of individual genetically defined serotonergic terminals in the CA1 in a behaving animal.

In order to visualize the locomotion- and reward-related activity of these fibers, we used a head-fixed VR task (Sato et al., 2017) in which a water-restricted mouse moves through a virtual linear track by running on a wheel under a two-photon microscope. The animal can receive up to 3 drops of water reward (1 drop/s) delivered through a mouth straw on reaching a specific area of the track (Fig. 2*C*). If the animal leaves the reward zone prematurely, the second and/or third reward is not delivered. Thus, trained mice immediately slowed down on delivery of the reward and came to a full halt to maximize reward (the

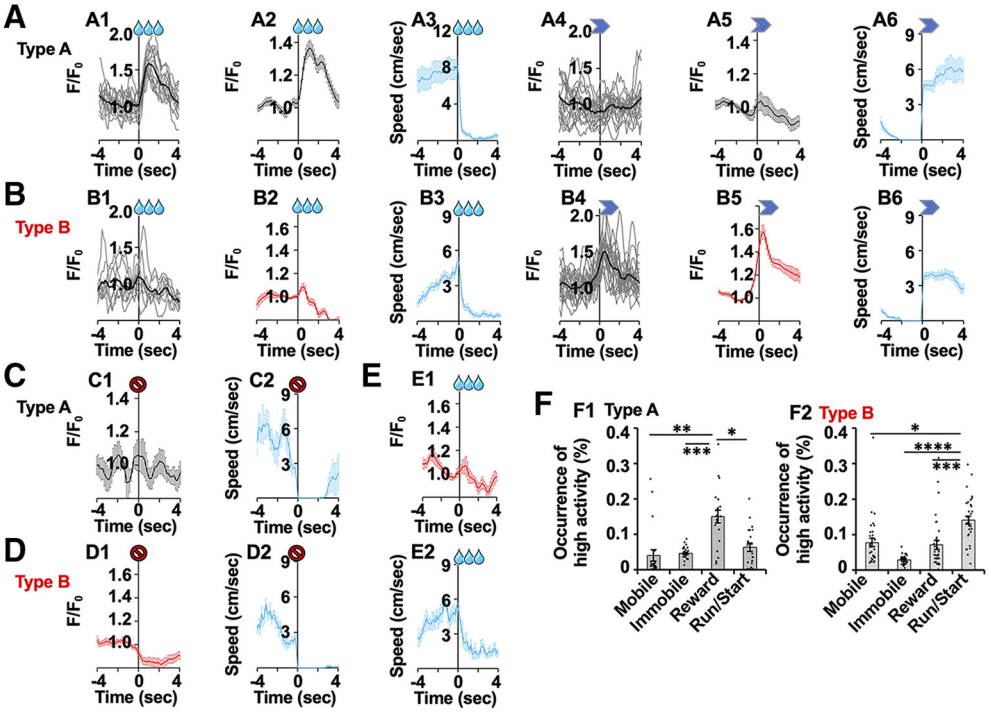

Figure 3. Dynamics of serotonergic fiber activity in CA1. ***A***, ***B***, Two populations of serotonergic fibers identified in hippocampal CA1 region. Type A: a reward-modulated fiber (***A***). Type B: locomotion-modulated fibers (***B***). Fluorescent intensity and running speed (blue) at reward delivery or run-start are shown. Example traces are shown with every individual reward and run-start instances taken from a single session (gray) and the average for that session (black) (***A1***,***B1***,***A4***,***B4***). The activity of the same fiber is shown at reward receipt and running start (one example fiber for Type A, one different example fiber for Type B). Averaged fluorescent activity (***A2***,***B2***,***A5***,***B5***) and running speed (***A3***,***B3***,***A6***,***B6***) of all fibers classified as Type A ($n = 21$ sessions from 3 animals) or Type B ($n = 32$ sessions from 4 animals) fibers are shown. Data were normalized by the baseline before the events (−3 to −1 s for run-start events and −2 −0 s for other events). ***A1***, ***A4***, Data were obtained from a single session from a mouse. The same applies to ***B1*** and ***B4***. ***C***, ***D***, Calcium activity at stopping of locomotion without receipt of reward (***C***, for Type A fibers, $n = 8$ sessions, 2 animals; ***D***, for Type B fibers, $n = 11$ sessions, 3 animals). ***E***, Calcium activity for Type B fibers averaged at instances of reward receipt that occurred without complete stop of locomotion ($n = 12$ sessions from 4 animals). ***F***, Distribution of peak activity within times of reward receipt, run-start, immobility, or locomotion. For Type A fiber, reward frames had significantly more peak activity than other groups (for Type A fiber, repeated-measures one-way ANOVA, $p < 0.05$ or lower, $n = 21$ sessions from 3 animals). For Type B fiber, run-start frames had significantly more peak activity than other groups (repeated-measures one-way ANOVA, $p < 0.05$ or lower, $n = 32$ sessions from 4 animals). Data are mean ± SEM. *$p < 0.05$; **$p < 0.01$; ***$p < 0.001$; ****$p < 0.0001$; repeated-measures one-way ANOVA.

time required to reach 50% of the speed at the reward delivery; 269 ± 49 ms, $n = 7$ mice). In most laps, mice successfully received at least one water reward (96 ± 3%, $n = 7$, day 7). Thereafter, the mice started moving again to complete the lap and were teleported back to the start of the track to resume a new lap (Fig. 2*D*).

Activity of GCaMP6f-expressing serotonergic fibers could be imaged in the stratum oriens of CA1 via the optical window (Fig. 2*E*). Seven serotonergic projection fibers from 7 animals could be successfully imaged for 3–7 d and were analyzed in depth. We found that these fibers showed either of two distinct patterns of response, although we do not rule out the existence of additional types of fibers whose activity was not detected under this task. Type A fibers displayed an increase in activity right after the animals received reward and ceased movement (Fig. 3*A1–A3*; paired two-tailed t test, $t_{(20)} = 7.841$, $p < 0.0001$, compared with reshuffled, $n = 21$ sessions from 3 animals). Activity then decayed as the reward delivery finished. In contrast, Type B fibers demonstrated pronounced activity at the start of a running bout (Fig. 3*B4-B6*; paired two-tailed t test, $t_{(31)} = 11.79$, $p < 0.0001$, compared with reshuffled, $n = 32$ sessions from 4 animals).

Type A fibers did not fire when animals stopped at an unrewarded position, indicating that activity is not due to halting (Fig. 3*C*, top; $N = 8$ sessions, 2 animals). Further, in contrast to Type B fibers, the fluorescence change at run-start was close to zero (Fig. 3*A4–A6*; paired two-tailed t test, $t_{(20)} = 0.5079$, $p = 0.617$, fluorescence change in data compared with reshuffled, $n = 21$ total sessions from 3 animals). Quantitative comparison of fluorescence increase shows a significant difference between reward receipt and run-start (first 2 s after event, repeated-measures two-way ANOVA, $F_{(1,300)} = 56.10$, $p < 0.0001$, $n = 21$ sessions from 3 animals).

The activity of Type B fibers peaked within 0.49 ± 0.04 s after the onset of locomotion, then gradually reduced to the basal level as the animal reached a steady speed (Fig. 3*B4-B6*; for details, see Materials and Methods). Type B fibers did not show activity at the delivery of reward (paired two-tailed t test, $t_{(31)} = 1.053$, $p = 0.3005$, fluorescence increase in data compared with reshuffled, $n = 32$ total sessions from 4 animals; Fig. 3*B1-B3*). Quantitative comparison of fluorescence change from the baseline shows asignificant difference between run-start and reward receipt (first 2 s after event, repeated-measures two-way ANOVA, $F_{(1,465)} = 309.7$, $p < 0.0001$, $n = 32$ sessions from 4 animals). There was rather a slight reduction in activity, which can be explained by locomotory effects, as the mice halt following reward receipt to drink (Fig. 3*D*). Indeed, when we analyze the data using instances when reward receipt did not come to a full locomotion halt, the decrease in fluorescence following reward for Type B fibers becomes less pronounced ($n = 12$ sessions from 4 animals; Fig. 3*E*).

None of the observed fibers displayed a mixed pattern of activity; for all 7 observed fibers, the overall fluorescence change in

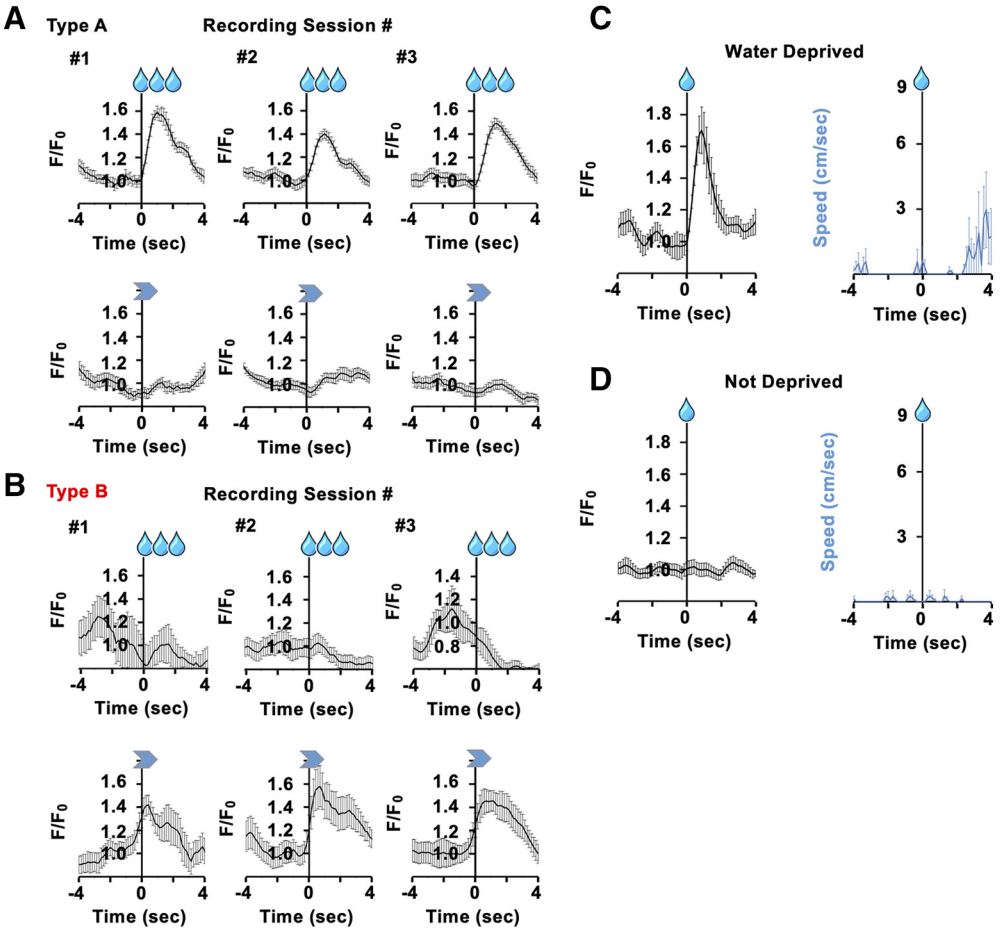

Figure 4. Stability of the fiber activity and dependency to the reward. ***A***, ***B***, Representative trace of Type A and B fiber activity over consecutive days of imaging. The trace was averaged across events in the same day. ***C***, Type A fiber activity to single unpredicted reward delivered in the absence of VR, randomly delivered while the animal is immobile. Black represents calcium activity. Blue represents speed. ***D***, The same fiber but imaged 1 d later after the animal was given free access to water for 1 d and no longer thirsty. Data are mean ± SEM.

response to run-start was significantly different from change to the reward event (repeated-measures two-way ANOVA interactions between groups, $p < 0.0001$ for each of the 7 fibers individually; for all 3 Type A fibers combined, $F_{(1,404)} = 187.6$, $p < 0.0001$; for all 4 Type B fibers combined, $F_{(1,681)} = 207.3$, $p < 0.0001$). We analyzed the distribution of peaks (Fig. 3*F*) within reward, run-start, and period of mobility or immobility (excluding run-start/reward, peaks defined as top 5% of activity; see Materials and Methods). The result shows that the highest activity was concentrated around reward for Type A fibers (repeated-measures one-way ANOVA, $F_{(1.787,35.74)} = 12.85$, $p = 0.0001$; *post hoc* reward vs mobile, $t_{(20)} = 4.256$, $p = 0.0002$; vs immobile $t_{(20)} = 5.23$, $p = 0.0023$; vs run-start, $t_{(20)} = 3.265$, $p = 0.023$, Sidak's correction, $n = 21$ sessions from 3 animals) and start of locomotion for Type B fibers (repeated-measures one-way ANOVA, $F_{(2.209,68.48)} = 17.63$, $p < 0.0001$; *post hoc* run-start vs mobile, $t_{(31)} = 3.247$, $p = 0.0167$; vs immobile $t_{(31)} = 9.817$, $p < 0.0001$; vs reward $t_{(31)} = 4.602$, $p = 0.0004$, Sidak's correction, $n = 32$ sessions from 4 animals).

Reward fiber identity is stable across days and responds to reward magnitude

The fibers demonstrated stable activity across several days of recordings, retaining their activity pattern observed on the first day (Fig. 4*A*,*B*). These results demonstrate the presence of a heterogeneous pool of serotonergic inputs into the CA1, with at least two patterns of activity, one related to reward and a second related to locomotion, that maintain the same signal across time.

In order to test whether Type A fibers respond to the value of the reward, we tested whether the reward-response was still present if the animal was given unpredicted reward while it is not moving. A reliable increase of the activity of Type A fibers was still detected (Fig. 4*C*), and the increase was dependent on the animal being water-deprived (Fig. 4*D*). We also wondered whether Type A fibers show an early increase in activity preceding the reward, relevant for reward prediction or reward prediction error (Schultz, 1997). Such activity was not detected (Fig. 3*A1*,*A2*) unlike dopaminergic neurons in ventral tegmental area; thus, the Type A fibers have a distinct function. The increase of fiber activity is related to the reward receipt itself and not to the reward expectation or the halt of locomotion. In contrast, the activation of Type B fibers preceded the initiation of locomotion by 0.63 ± 0.06 s (Fig. 3*B4*,*B5*; $n = 32$ sessions from 4 animals), suggesting that this response reflects the animal's action planning.

We then decided to explore whether A fibers carry any quantitative evaluation of the reward magnitude. As such, we analyzed the magnitude of response during the repeated laps as the animals were gradually sated and the reward devalues. We detected a statistically significant decline of the intensity of Ca^{2+} response as the animal collected more rewards (Fig. 5*A*; Pearson correlation, $p = 0.0451$, $R^2 = 0.2742$, $n = 21$ sessions from 3 animals). Moreover, the reward-elicited increase in activity was

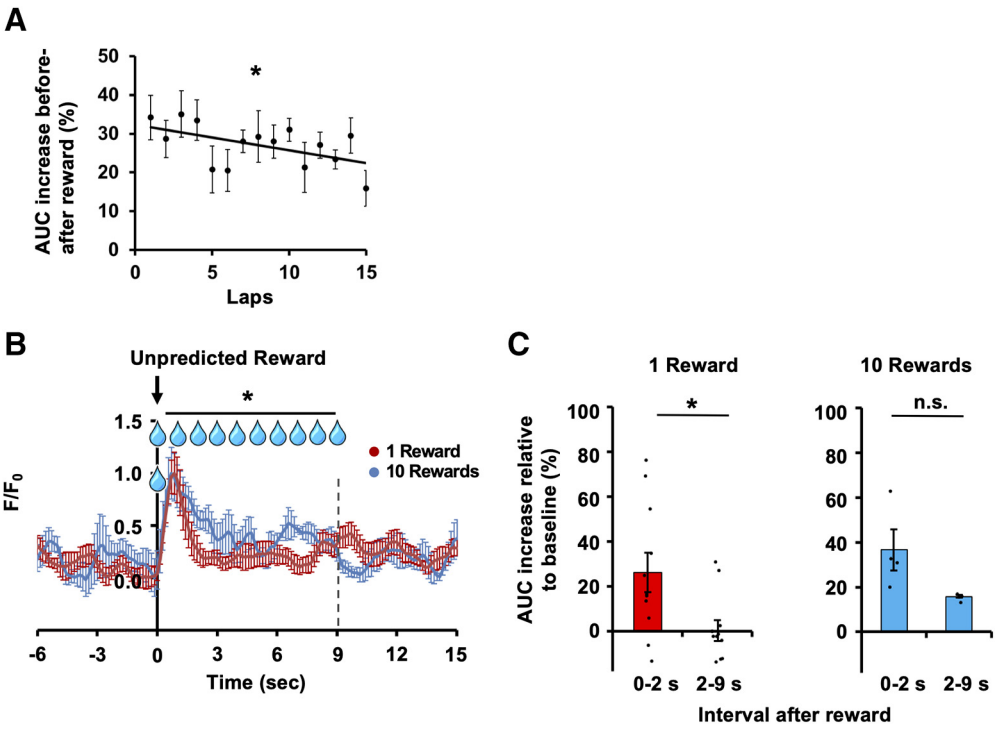

Figure 5. Quantitative effects of multiple rewards on reward fiber dynamic. ***A***, Type A fiber activity dynamic as animals collect more rewards within the same session. Pearson correlation, $p = 0.0451$ ($n = 21$ sessions from 3 animals). ***B***, Averaged reward activity of a Type A fiber when 10 drops of reward (blue) or single-drop reward (red) were given. Repeated-measures two-way ANOVA (interaction between 1-drop and 10-drops groups significant after the peak, $p = 0.0346$, $n = 11$ reward events for 1-reward group, $n = 4$ reward events for 10-rewards group) from two different sessions in the same mouse. ***C***, Quantitative assessment of fluorescence in the 0-2 and 2-9 s interval relative to a baseline for the 1-drop trace ($p = 0.0327$, paired t test, $n = 11$ events) and 10-drops trace ($p = 0.0988$, paired t test, $n = 4$ events). Data are mean ± SEM. *$p < 0.05$. n.s., not significant.

sustained during the delivery of multiple rewards (10 water drops over 9 s), compared with 1 reward delivery (Fig. 5*B*; repeated-measures two-way ANOVA, interaction between groups and time significant after the peak, $F_{(1,13)} = 5.567$, $p = 0.0346$, $n = 11$ reward events for 1-reward group, $n = 4$ reward events for 10-rewards group, from two different sessions in the same mouse). We quantitatively compared the 2–9 s interval against the peak preceding it (0–2 s after reward receipt) and subtracting the average of 10 s preceding the reward delivery. Sustained activity was significantly lower than the peak that precedes it in the 1-drop trace (Fig. 5*C*; paired two-tailed t test, $t_{(10)} = 2.478$, $p = 0.0327$, $n = 11$ events), but not in the 10-drops trace (paired two-tailed t test, $t_{(3)} = 2.366$, $p = 0.0988$, $n = 4$ events).

Serotonergic input into CA1 is required for shaping reward-induced behavior

The evidence from our *in vivo* imaging suggests a possible role of serotonergic input in the transmission of reward information to the hippocampus. In order to test whether activity of hippocampal serotonergic fiber shapes reward-related behavior, we used an optogenetic approach locally in dorsal hippocampus. Given that two different types of fibers coexist in the CA1 region, Type A fibers activated on reward delivery and Type B activated when the animals resume running (Fig. 3*A*,*B*), we decided to inhibit the activity of all fibers specifically when the animals occupied the reward delivery zone, with the expectation that this inhibition would disrupt the temporal structure of the activation. We crossed the *Sert-Cre* mouse line with a Cre-dependent line-expressing NpHR (*Sert-Cre/Ai39D*) (Madisen et al., 2012) and implanted optic fibers in dorsal CA1 to target the fiber terminals (Fig. 6*A*). As a control, we used littermates not expressing light-sensitive channels. Light was delivered while animals were inside the reward zone (Fig. 6*B*).

Inhibition of the CA1 serotonergic projections led to impaired performance, including a significant increase in errors (defined as laps without full collection of all three rewards; inhibited 24.2 ± 5.6% vs control 5.8 ± 2.6%, unpaired two-tailed t test, with Welch's correction $t_{(45.35)} = 3.005$, $p = 0.0043$, $n = 34$ sessions for transgenics and 23 sessions from controls, pooled from the 5 d duration of the task, from 7 transgenic mice and 5 control animals; Fig. 6*C*) and a decrease of rewards collected per lap (inhibited 2.71 ± 0.07 vs control 2.94 ± 0.03, unpaired two-tailed t test, with Welch's correction, $t_{(44.07)} = 2.953$, $p = 0.0050$, $n = 34 + 23$ sessions; Fig. 6*D*). Distribution of time spent per section of the linear track also differed between the two groups. Inhibited animals spent less time within the reward zone (repeated-measures two-way ANOVA interaction, $F_{(19,1045)} = 2.076$, $p = 0.0044$, *post hoc* comparison with Sidak's correction for reward bin, $t_{(1100)} = 4.666$, $p = 0.0001$, $n = 34 + 23$ sessions; Fig. 6*E*) and had overall shorter halt duration in the rewarded area per lap (inhibited 6.46 ± 0.61 s vs control 9.69 ± 0.93 s, unpaired two-tailed t test, $t_{(55)} = 3.044$, $p = 0.0036$, $n = 34 + 23$ sessions; Fig. 6*F*).

Discussion

Remembering, locating, and exploring rewarded locations are fundamental to an animal's survival. Our data suggest ways in which reward-triggered activity in the median raphe may lead to behavioral changes via modulation of the hippocampal CA1 region. Furthermore, the diverse activity of the axonal fibers we described supports a way that the serotonergic system can allow the CA1 to integrate both locomotion signals as well as signals related to rewarded locations.

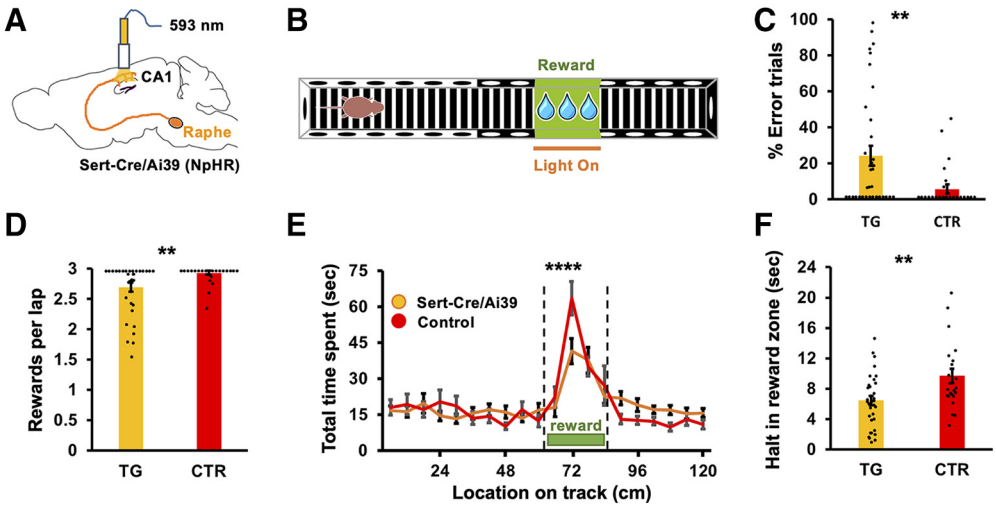

Figure 6. Inhibition of serotonergic fiber in CA1 modifies reward-induced behavior. ***A***, ***B***, Experimental settings. Optic cannulas were implanted bilaterally over dorsal hippocampal CA1 regions in transgenic mice expressing NpHR in serotonergic neurons. ***C***, Percentage of errors during the performance of the virtual linear track task. Inhibition of CA1 serotonergic fibers significantly increased the number of errors (*t* test, $p < 0.01$, $n = 34$ sessions for transgenics [TG] and 23 sessions from controls [CTR], pooled from the 5 d duration of the task, from 7 transgenic mice and 5 control animals). ***D***, Effect of the optogenetic inhibition on the reward collection performance. Inhibition of the serotonergic fibers in CA1 reduced the average number of rewards collected per lap (*t* test, $p < 0.01$, $n = 34$ sessions for transgenics and 23 sessions from controls, pooled from the 5 d duration of the task, from 7 transgenic mice and 5 control animals). ***E***, Occupancy in the virtual linear track. Inhibition of serotonergic fibers in CA1 caused a reduction of time spent in the rewarded area (two-way repeated-measures ANOVA interaction, $p < 0.01$, *post hoc* test, $p < 0.0001$ for reward bin). ***F***, Average halt per lap in reward zone. CA1 serotonergic fiber inhibition resulted in shorter halting in the reward zone compared with control animals (*t* test, $p < 0.01$, $n = 34$ sessions for transgenics and 23 sessions from controls, pooled from the 5 d duration of the task, from 7 transgenic mice and 5 control animals). Data are mean ± SEM. $^{**}p < 0.01$, $^{****}p < 0.0001$.

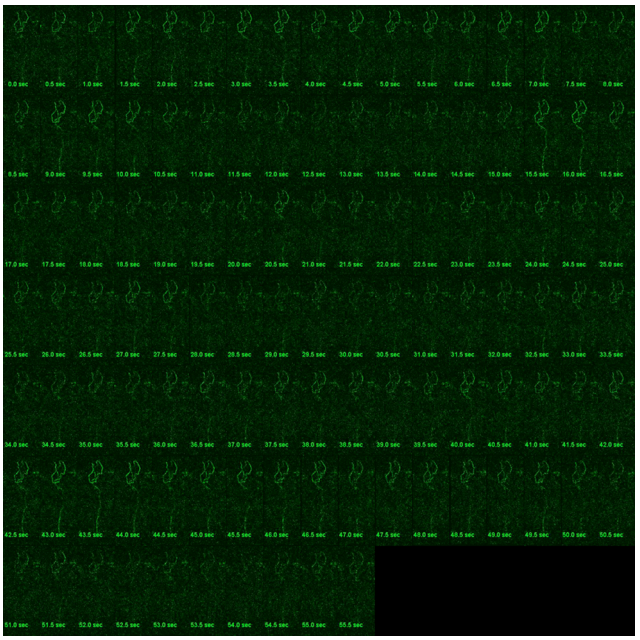

Movie 1. Example two-photon microscopic images of a serotonergic fiber in hippocampal CA1 region in a behaving mouse. This fiber belonged to Type B. The recording was performed at 50 μm below the alveus at 2 Hz. [View online]

We first show that serotonergic innervation in the dorsal CA1 can be classified into two functionally distinct activity patterns. Type A fibers fire after reward receipt, but not when animals stop in an unrewarded area. In contrast, Type B fibers fire when animals initiate locomotion. Because firing of Type A fibers was observed even when the animal was given reward when it was not running and also the firing were not associated with spontaneous stopping (Fig. 3*C*), we reasoned that the activity of Type A fiber activity is not simply a "stop here" signal but rather conveys information concerning reward receipt and modulates the stationary period.

Previous studies have shown that inputs from the raphe preferentially synapse on various classes of interneurons in the hippocampus, many of which are known to be dendrite targeting and disinhibitory (Papp et al., 1999; Varga et al., 2009). Of particular interest, vasoactive intestinal peptide interneurons are one of the downstream targets of median raphe projections and have been shown to exhibit locomotion-modulated and reward-modulated activity in CA1 *in vivo* (Turi et al., 2019). Furthermore, serotonin in the hippocampus has been linked with increased plasticity (Lesch and Waider, 2012; Fernandez et al, 2017; Teixeira et al, 2018). Combined with our findings, we could speculate that activation of a population of serotonergic fibers in the hippocampus at the time of reward might transiently increase the likelihood of pyramidal cell cofiring and subsequent synaptic plasticity. Therefore, the observed serotonergic signal may be the basis for the formation and consolidation of reward cells in CA1(Gauthier and Tank, 2018). Future studies are likely to explore this possibility, as well as the role of other populations of serotonergic fibers in the hippocampus.

Median raphe is the major source of hippocampal serotonergic fibers (Kohler and Steinbusch, 1982; Papp et al., 1999; Vertes et al, 1999; Varga et al, 2009; Turi et al., 2019). In addition, the caudal and interfascicular subnucleus of the dorsal raphe also projects to the hippocampus (Vertes, 1991; McKenna and Vertes, 2001; Izawa et al., 2019). Single-cell transcriptome and lineage analyses have found that there is heterogeneity among serotonergic neuronal cell types, identifying at least four in median raphe and also four in dorsal raphe (Okaty et al, 2015). Among those, *Egr2-Pet1*-positive neurons and *Rse2(Hoxa2)-Pet1*-positive neurons in median raphe both project to hippocampus. Notably, *Rse2(Hoxa2)-Pet1*-positive neurons coexpress vesicular glutamate transporter vGluT3 and corelease glutamate along with serotonin (Szőnyi et al, 2016). Future studies using

specific *Cre* line are required to test which subpopulation represents which fiber type and also to identify the exact transmitter used in the behavioral modulation as described above.

In conclusion, our work provides new insight on the serotonergic input activity within the CA1 and on how this pathway could connect reward and behavioral changes during learning.

References

Azmitia EC, Segal M (1978) An autoradiographic analysis of the differential ascending projections of the dorsal and median raphe nuclei in the rat. J Comp Neurol 179:641–667.

Domonkos A, Nikitidou Ledri L, Laszlovszky T, Cserep C, Borhegyi Z, Papp E, Nyiri G, Freund TF, Varga V (2016) Divergent in vivo activity of non-serotonergic and serotonergic VGluT3-neurones in the median raphe region. J Physiol 594:3775–3790.

Dugue GP, Lorincz ML, Lottem E, Audero E, Matias S, Correia PA, Lena C, Mainen ZF (2014) Optogenetic recruitment of dorsal raphe serotonergic neurons acutely decreases mechanosensory responsivity in behaving mice. PLoS One 9:e105941.

Eichenbaum H (2000) A cortical-hippocampal system for declarative memory. Nat Rev Neurosci 1:41–50.

Fernandez SP, Muzerelle A, Scotto-Lomassese S, Barik J, Gruart A, Delgado-García JM, Gaspar P (2017) Constitutive and acquired serotonin deficiency alters memory and hippocampal synaptic plasticity. Neuropsychopharmacology 42:512–523.

Gauthier JL, Tank DW (2018) A dedicated population for reward coding in the hippocampus. Neuron 99:179–193.e177.

Gong S, Zheng C, Doughty ML, Losos K, Didkovsky N, Schambra UB, Nowak NJ, Joyner A, Leblanc G, Hatten ME, Heintz N (2003) A gene expression atlas of the central nervous system based on bacterial artificial chromosomes. Nature 425:917–925.

Ihara N, Ueda S, Kawata M, Sano Y (1988) Immunohistochemical demonstration of serotonin-containing nerve fibers in the mammalian hippocampal formation. Acta Anat (Basel) 132:335–346.

Izawa S, Miki K, Tsuchiya M, Yamada H, Nagayama M (2019) Hair and fingernail cortisol and the onset of acute coronary syndrome in the middle-aged and elderly men. Psychoneuroendocrinology 101:240–245.

Jackson J, Dickson CT, Bland BH (2008) Median raphe stimulation disrupts hippocampal theta via rapid inhibition and state-dependent phase reset of theta-related neural circuitry. J Neurophysiol 99:3009–3026.

Kocsis B, Varga V, Dahan L, Sik A (2006) Serotonergic neuron diversity: identification of raphe neurons with discharges time-locked to the hippocampal theta rhythm. Proc Natl Acad Sci USA 103:1059–1064.

Kohler C, Steinbusch H (1982) Identification of serotonin and non-serotonin-containing neurons of the mid-brain raphe projecting to the entorhinal area and the hippocampal formation: a combined immunohistochemical and fluorescent retrograde tracing study in the rat brain. Neuroscience 7:951–975.

Lesch KP, Waider J (2012) Serotonin in the modulation of neural plasticity and networks: implications for neurodevelopmental disorders. Neuron 76:175–191.

Li Y, Zhong W, Wang D, Feng Q, Liu Z, Zhou J, Jia C, Hu F, Zeng J, Guo Q, Fu L, Luo M (2016) Serotonin neurons in the dorsal raphe nucleus encode reward signals. Nat Commun 7:10503.

Liu Z, Zhou J, Li Y, Hu F, Lu Y, Ma M, Feng Q, Zhang JE, Wang D, Zeng J, Bao J, Kim JY, Chen ZF, El Mestikawy S, Luo M (2014) Dorsal raphe neurons signal reward through 5-HT and glutamate. Neuron 81:1360–1374.

Madisen L, Mao T, Koch H, Zhuo J, Berenyi A, Fujisawa S, Hsu YW, Garcia AJ, Gu X, Zanella S, Kidney J, Gu H, Mao Y, Hooks BM, Boyden ES, Buzsáki G, Ramirez JM, Jones AR, Svoboda K, Han X, et al. (2012) A toolbox of Cre-dependent optogenetic transgenic mice for light-induced activation and silencing. Nat Neurosci 15:793–802.

McKenna JT, Vertes RP (2001) Collateral projections from the median raphe nucleus to the medial septum and hippocampus. Brain Res Bull 54:619–630.

Miyazaki KW, Miyazaki K, Tanaka KF, Yamanaka A, Takahashi A, Tabuchi S, Doya K (2014) Optogenetic activation of dorsal raphe serotonin neurons enhances patience for future rewards. Curr Biol 24:2033–2040.

Ohmura Y, Tanaka KF, Tsunematsu T, Yamanaka A, Yoshioka M (2014) Optogenetic activation of serotonergic neurons enhances anxiety-like behaviour in mice. Int J Neuropsychopharmacol 17:1777–1783.

Okaty BW, Freret ME, Rood BD, Brust RD, Hennessy ML, deBairos D, Kim JC, Cook MN, Dymecki SM (2015) Multi-scale molecular deconstruction of the serotonin neuron system. Neuron 88:774–791.

Papp EC, Hajos N, Acsady L, Freund TF (1999) Medial septal and median raphe innervation of vasoactive intestinal polypeptide-containing interneurons in the hippocampus. Neuroscience 90:369–382.

Paxinos G, Franklin KBJ (2004) The mouse brain in stereotaxic coordinates, Ed 2. Amsterdam: Elsevier.

Sato M, Kawano M, Mizuta K, Islam T, Lee MG, Hayashi Y (2017) Hippocampus-dependent goal localization by head-fixed mice in virtual reality. eNeuro 4:ENEURO.0369-16.2017.

Schultz W (1997) Dopamine neurons and their role in reward mechanisms. Curr Opin Neurobiol 7:191–197.

Sos KE, Mayer MI, Cserép C, Takács FS, Szőnyi A, Freund TF, Nyiri G (2017) Cellular architecture and transmitter phenotypes of neurons of the mouse median raphe region. Brain Struct Funct 222:287–299.

Szőnyi A, Mayer MI, Cserép C, Takács VT, Watanabe M, Freund TF, Nyiri G (2016) The ascending median raphe projections are mainly glutamatergic in the mouse forebrain. Brain Struct Funct 221:735–751.

Teixeira CM, Rosen ZB, Suri D, Sun Q, Hersh M, Sargin D, Dincheva I, Morgan AA, Spivack S, Krok AC, Hirschfeld-Stoler T, Lambe EK, Siegelbaum SA, Ansorge MS (2018) Hippocampal 5-HT input regulates memory formation and Schaffer collateral excitation. Neuron 98:992–1004.e4.

Turi GF, Li WK, Chavlis S, Pandi I, O'Hare J, Priestley JB, Grosmark AD, Liao Z, Ladow M, Zhang JF, Zemelman BV, Poirazi P, Losonczy A (2019) Vasoactive intestinal polypeptide-expressing interneurons in the hippocampus support goal-oriented spatial learning. Neuron 101:1150–1165.e1158.

Varga V, Losonczy A, Zemelman BV, Borhegyi Z, Nyiri G, Domonkos A, Hangya B, Holderith N, Magee JC, Freund TF (2009) Fast synaptic subcortical control of hippocampal circuits. Science 326:449–453.

Vertes RP (1991) A PHA-L analysis of ascending projections of the dorsal raphe nucleus in the rat. J Comp Neurol 313:643–668.

Vertes RP, Fortin WJ, Crane AM (1999) Projections of the median raphe nucleus in the rat. J Comp Neurol 407:555–582.

Wang DV, Yau HJ, Broker CJ, Tsou JH, Bonci A, Ikemoto S (2015) Mesopontine median raphe regulates hippocampal ripple oscillation and memory consolidation. Nat Neurosci 18:728–735.